

Available online at [www.sciencedirect.com](http://www.sciencedirect.com)**ScienceDirect**

Procedia Engineering 204 (2017) 194–201

**Procedia  
Engineering**[www.elsevier.com/locate/procedia](http://www.elsevier.com/locate/procedia)

14th Hypervelocity Impact Symposium 2017, HVIS2017, 24-28 April 2017, Canterbury, Kent,  
UK

# A Study of the effect of aspect ratio on fragmentation of explosively driven cylinders

Tom De Vuyst<sup>\*,a</sup>, Rade Vignjevic<sup>a</sup>, James C. Campbell<sup>a</sup>, Andreas Klavzar<sup>b</sup>, Marina Seidl<sup>b</sup>

<sup>a</sup>*Dynamic Response Group, Structural Integrity, Institute of Materials and Manufacturing, Brunel University London, Grant Park, NSIRC, Great Abington, Cambridge, CB21 6AL, UK.*

<sup>b</sup>*French-German Research Institute of Saint-Louis, 5 rue du Général Cassagnou, 68300 Saint-Louis, France*

---

## Abstract

The work presented in this paper consists of a parametric study of explosively driven fracture and fragmentation of steel cylinders. The effect of cylinder height to wall thickness ratio on the failure mode and fragment shape is studied using a numerical model based on the meshless Smoothed Particle Hydrodynamics (SPH) method. The simulation results are supplemented with experiments with identical charge geometries and materials, to analyse the natural fragmentation behaviour of the different cylinders. Characteristic fragments were softly recovered in a water basin and fragment mass distributions are compared to the simulation results.

© 2017 The Authors. Published by Elsevier Ltd.

Peer-review under responsibility of the scientific committee of the 14th Hypervelocity Impact Symposium 2017.

*Keywords:* explosively driven cylinders; fragmentation; dynamic fracture; smoothed particle hydrodynamics; soft recovery;

---

## 1. Introduction

The effect of cylinder aspect ratio on the fragment shape and failure mode has been observed in electromagnetically driven expansion of aluminium rings [1], and has also been reported for Ti-6Al-4V in [2]. For

---

\* Corresponding author. Tel.: +441223940100; fax: +0-000-000-0000 .  
E-mail address: [tom.devuyst@brunel.ac.uk](mailto:tom.devuyst@brunel.ac.uk)

**Nomenclature**

$\delta$	Kernel smoothing length
$\varepsilon_0$	Reference strain rate
$\dot{\varepsilon}$	Effective strain rate
$\bar{\varepsilon}_{pl}$	Effective plastic strain
$\nu$	Poisson's ratio
$\rho_a$	Particle a density
$\sigma$	Stress
$\sigma_{eq}$	Von Mises stress
$\sigma_Y$	Flow stress
$d_i$	Cylinder inner diameter
$d_o$	Cylinder outer diameter
$e$	Internal energy
$h$	Cylinder height
$m_a$	Particle a mass
$p$	Pressure
$w$	Cylinder wall thickness
$x_a$	Particle a position
$D$	Damage
$\dot{D}$	Damage rate
$E$	Young's modulus
$W$	Kernel function
$T$	Temperature
$T^*$	Homologous temperature

ductile materials and a 1:1 aspect ratio diffuse necking dominates [1], while for larger aspect ratios shear bands occur. For longer cylinders with aspect ratio of the order of 1:10, the fragments tend to be elongated along the cylinder axis. This observation was already made by Mott in 1947 [3]. In this paper the explosively driven fragmentation of EN 34CrNiMo6 study steel cylinders are studied. Similar to the experiments performed by Mock and Holt [4] on cylinders of Armco iron and HF1 steel, the cylinders are filled with explosive to drive the radial expansion and fracture of the cylinders (see Fig 1). In the current study the wall thickness to height ratio of the cylinders is varied in the range 1:1 to 1:10, and the effect of this change in aspect ratio on the fracture and fragmentation is studied. Numerical simulations using the meshless Smoothed Particle Hydrodynamics (SPH) method were performed and these simulation results are supplemented with experiments with identical charge geometries and materials, to analyse the natural fragmentation behaviour of the different charges. Characteristic fragments were softly recovered in a water basin.

## 2. Experiments

### 2.1. Steel cylinder dimension and material

The experimental setup consists of placing the hollow steel cylinders over the explosive charge (Fig. 1). The outer diameter  $d_o$  and inner diameter  $d_i$  of the steel cylinders are the same for all conducted experiments. Keeping the cylinder wall thickness  $w$  constant, different cylinder heights  $h$  were tested. The cylinder height  $h$  was taken as a

multiple of wall thickness  $w$ , to test the influence of cylinder height to thickness ratio on the size and shape of generated fragment. Four  $w/h$  ratios were defined for (Table 1).

Table 1 Charge and steel cylinder dimension given in [mm]

$h/w$	$x_1$	$h$	$x_2$	$x$	$d_i$	$d_o$	$w$
1:1	45.0	9.5	32.0	86.5	38.1	57.2	9.5
2:1	45.0	19.0	32.0	96.0	38.1	57.2	9.5
3:1	45.0	28.5	32.0	105.5	38.1	57.2	9.5
10:1	45.0	95.0	32.0	172.0	38.1	57.2	9.5

The cylinders were manufactured from EN 34CrNiMo6 steel. The chemical composition of this steel is shown in Table 2

Table 2 Chemical composition of hollow steel cylinder materials

Grade	Number	Carbon %	Chrome %	Nickel %	Molybdenum %	HBW
EN34CrNiMo6	1.6582	0.34	1.59	1.6	0.22	253

2.2. Charge dimension

The charge was a cylindrical shaped composition B explosive and placed inside the hollow steel cylinder (Fig. 1). The charge length  $x$  is dependent on the cylinder height  $h$ . The length  $x$  resulted from a constant extension  $x_1$  to the front, where charge is initiated, the varying cylinder height  $h$  and an extension to the back  $x_2$ . The charge diameter is equivalent to the inner cylinder diameter  $d_i$  (Table 1).

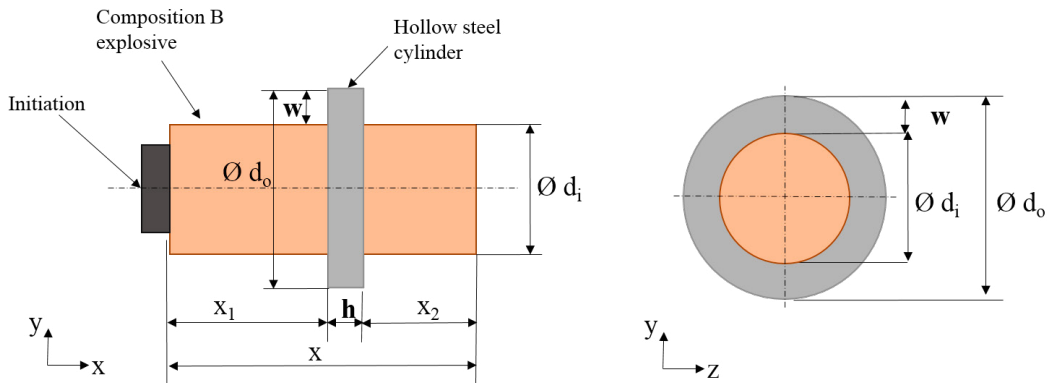


Fig. 1. Charge dimensions

2.3. Position

For soft fragment recovery, the charge was placed at a height  $y$  above a water basin (Fig. 2). As a consequence, only a fraction of the totally generated fragment mass is recovered. Due to symmetry conditions it is assumed, that the recovered fragments are good representatives in their size and shape of the characteristic fragments generated in the different tests.

From the charge geometry, the length  $l$  of the water surface and the distance of the charge from the water surface,

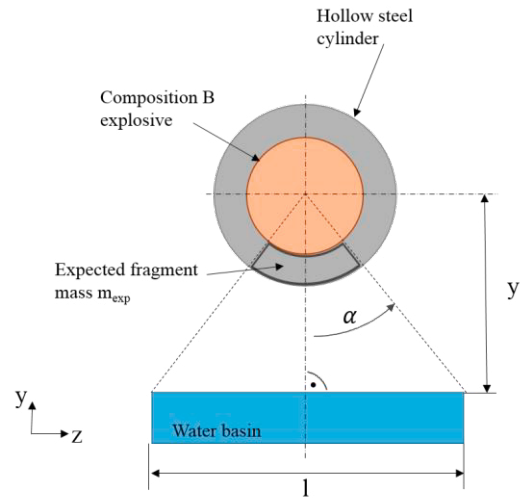
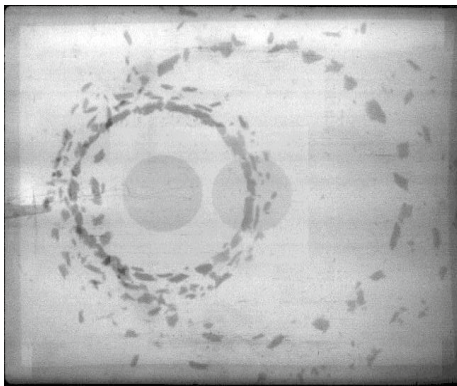
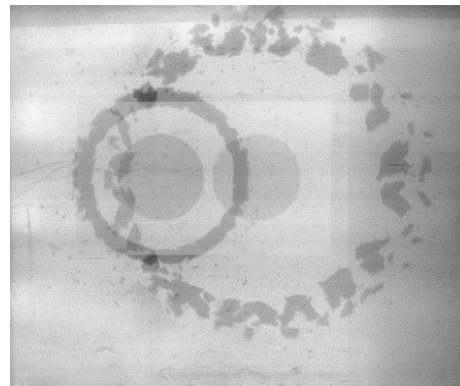


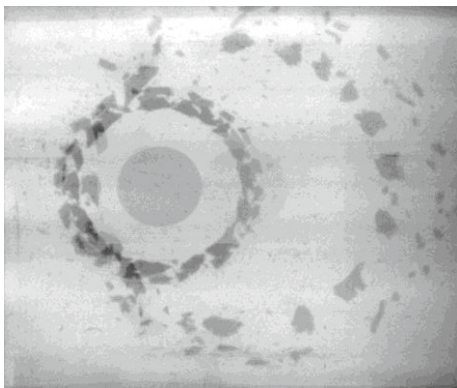
Fig. 2. Charge position and fragment recovery



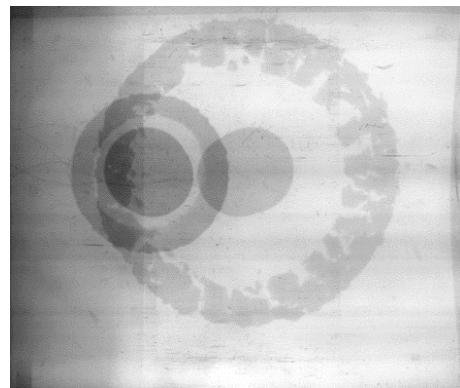
a)



b)



c)



d)

Fig. 3 Fragmentation of cylinders for a) 1:1, b) 1:2, c) 1:3 ratio and d) 1:10 cylinder aspect ratio

see Fig. 2, the expected fragment mass  $m_{exp}$  projected in the water basin can be calculated.

The recovered mass  $m_{rec}$  from the fragments found in the water basin is shown in relation to the initial cylinder mass  $m_{cyl}$  and to  $m_{exp}$  in Table 3. About an average 67 % from the expected recovered mass  $m_{exp}$  were recovered, giving an average from the recovered mass  $m_{rec}$  to the full cylinder mass  $m_{cyl}$  of about 20 %. The fragments can be observed in the double exposed X-ray images in Fig. 3.

Table 3 Expected and retrieved fragment masses

	h/w	y [mm]	l [mm]	$\alpha$ [deg]	$m_{cyl}$ [g]	$m_{exp}$ [g]	$m_{rec}$ [g]	Recovered from $m_{exp}$ %	Recovered overall %
A	1:1	690	1200	48.7	106	29	23	80	22
	1:1	720	1200	49.9	106	30	21	73	20
	2:1	710	1200	49.5	212	59	36	61	17
	3:1	720	1200	49.9	318	89	45	51	14
	10:1	710	1200	49.5	1060	293	179	61	17

### 3. Numerical Model

A numerical model was developed using the Smoothed Particle Hydrodynamics (SPH) method to discretise the geometry. Meshless methods, such as Smoothed Particle Hydrodynamics, are of particular interest for the prediction of fragmentation and fracture at high strain rate in metals as they are able to deal with large deformations, and propagation, bifurcation and joining of cracks. The method is also less sensitive to developing cracks along preferential directions (mesh sensitivity) than discretisations based on Finite Element Method (FEM).

The SPH method was developed by Lucy [5], and Gingold and Monaghan [6] for astro-physics problems and later extended to deal with solid mechanics problems by Libersky and Petschek et al. [7][8]. The form of the semi-discretized conservation equations used in this paper are:

$$\begin{aligned}
 \left\langle \frac{D\rho_i}{Dt} \right\rangle &= \rho_i \sum_{j=1} \frac{m_j}{\rho_j} (v_j - v_i) \nabla W(x_i - x_j, \delta) \\
 \left\langle \frac{Dv_i}{Dt} \right\rangle &= - \sum_{j=1} m_j \left( \frac{\sigma_j}{\rho_j^2} + \frac{\sigma_i}{\rho_i^2} \right) \nabla W(x_i - x_j, \delta) \\
 \left\langle \frac{DE_i}{Dt} \right\rangle &= - \frac{\sigma_i}{\rho_i} \sum_{j=1} m_j (v_j - v_i) \nabla W(x_i - x_j, \delta)
 \end{aligned}$$

The in-house developed SPH solver [9],[10] uses a central difference to integrate these conservation equations in time. The cylinder’s constitutive behavior was modelled using a modification of the Johnson-Cook strain rate and temperature dependent elasto-plasticity model:

$$\sigma_Y = (A + B\bar{\epsilon}_{pl}^n) \left( 1 + C \ln \left( \frac{\dot{\epsilon}}{\dot{\epsilon}_0} \right) + \left( \frac{\dot{\epsilon}}{D} \right)^E \right) (1 - T^{*m}) \tag{1}$$

This model was combined with a Lemaitre damage model:

$$\begin{aligned}
 \dot{D} &= \left( -\frac{Y}{S} \right)^t \dot{\epsilon}_{pl} & \text{if } \bar{\epsilon}_{pl} \geq \bar{\epsilon}_{threshold} \\
 \dot{D} &= 0 & \text{if } \bar{\epsilon}_{pl} < \bar{\epsilon}_{threshold}
 \end{aligned} \tag{2}$$

with

$$-Y = \frac{\sigma_{eq}^2}{2E(1-D)^2} \left( \frac{2}{3}(1+\nu) + 3(1-2\nu) \left( \frac{-p}{\sigma_{eq}} \right)^2 \right) \quad (3)$$

and a Grüneisen equation-of-state (EOS) [11].  $A, B, C, D, E, m, n, S, t$  are material parameters. Using this type of material model for the cylinder material is required because during the fragmentation process the cylinder is subjected to very complex loading. This loading consists of a combination of shockwaves and tensile hoop stresses due to the interaction with the explosive and the resulting high strain rate radial expansion, adiabatic heating and damage development leading to fractures. Material parameters for 4340 steel, the AISI equivalent of the EN 34CrNiMo6 studied in this paper, were used. The explosive was modelled using a high-explosive burn model with a JWL equation-of-state [10]. All models used a discretization with 10 particles through the cylinder wall resulting in approximately 67000, 205000, 242000 and 463000 particles for the 1:1, 1:2, 1:3 and 1:10 ratios respectively.

#### 4. Results

The simulation results are processed to identify individual fragments and their mass (see Fig. 4). In Fig. 4 each fragment calculated is given a different color, and the fragments are shown in their initial undeformed configuration.

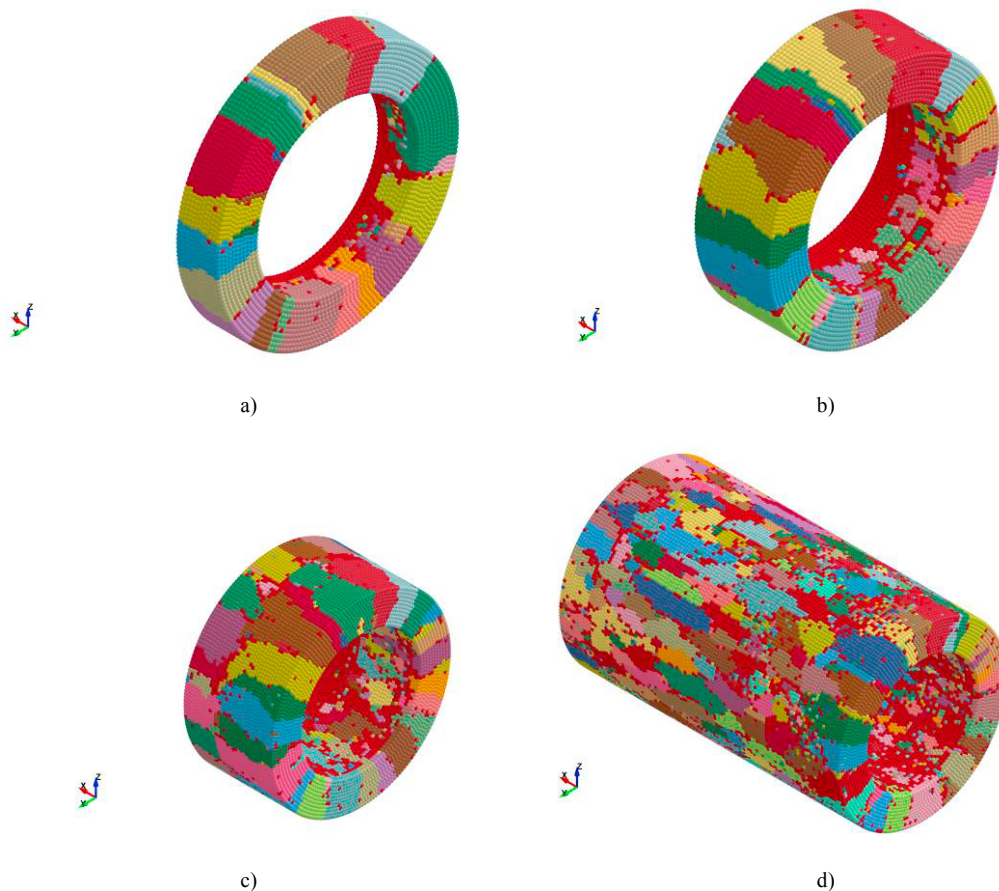


Fig. 4 Numerically predicted fragments for a) 1:1, b) 1:2, c) 1:3 and d) 1:10 cylinder aspect ratio

It can be seen that for the 1:1 and 1:2 aspect ratios the fractures mostly run along the full length of the cylinder, while for the 1:3 the numerical model predicts a fracture in the tangential direction, resulting in two fragments along the length of the cylinder. The recovered fragments from this test showed that many fragments still covered the whole height of the cylinder (see X-ray image in Fig. 3c). For the 1:10 aspect ratio the cylinder fragments in elongated fragments, with some more compact fragments towards the ends of the cylinder. These more compact fragments are also visible on the X-ray image in Fig. 3d.

Fig. 5 shows the distribution of fragment mass. The abscissa of the graph plot the fragment mass  $M$ , and the ordinates are the number of fragments with a mass less than fragment mass  $M$ . The predicted fragment mass distributions follow the same trends as the experimental results, except for the 1:1 aspect ratio where the simulation over predicts the fragment mass. The simulation results predict that for the 1:1, 1:2, 1:3 and 1:10 aspect ratios the largest fragments are 13.3, 14.5, 13.4, 11.8g. With the exception of the 1:1 ratio this compares well the experiments 3.7, 10.4, 13.3 and 13.3.

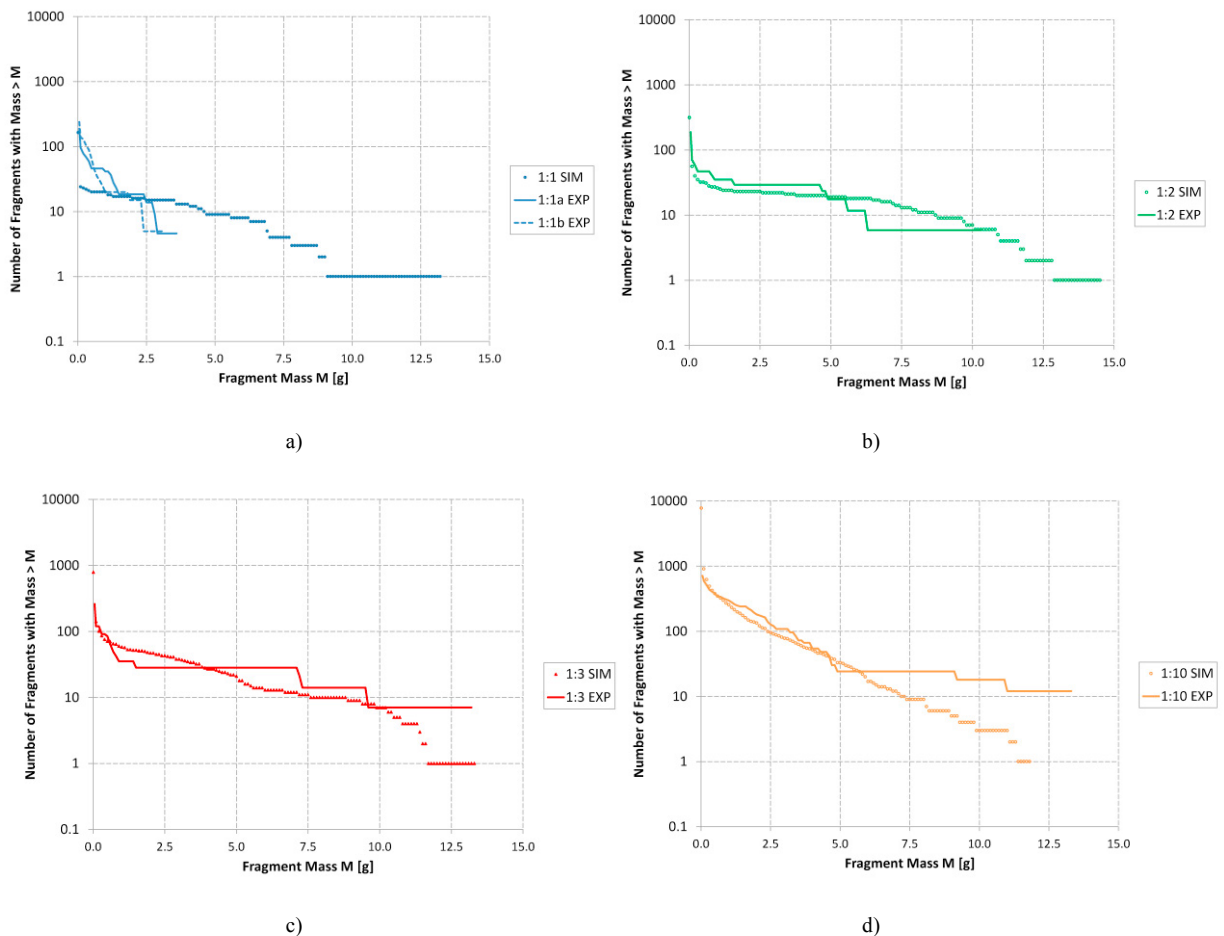


Fig. 5 Fragment mass results for a) 1:1, b) 1:2, c) 1:3 and d) 1:10 cylinder aspect ratio

## 5. Conclusions

The fragmentation of EN 34CrNiMo6 steel cylinders with different wall thickness to height ratios is studied in this paper. Four ratios, 1:1, 1:2, 1:3 and 1:10 were tested and simulated using the SPH method. For the ratios 1:1, 1:2 and 1:3 fragments run along the full length of the cylinder. The numerical model only predicts this for the 1:1 and 1:2 ratios. The 1:10 ratio results in a combination of elongated and more compact fragments, which is also predicted by the numerical model. The maximum fragment mass is predicted quite well for the 1:2, 1:3 and 1:10 ratios, while for the 1:1 ratio the predicted fragment mass is larger than the observed one. The discrepancy could be explained by the accuracy of the material models or the material parameters used; the numerical model used parameters for 4340 steel. Another source of error could be that improvements are required to the handling of failure and development fractures in the SPH method.

## References

- [1] Zhang, H. and Ravi-Chandar, K., On the dynamics of necking and fragmentation---II. Effect of material properties, geometrical constraints and absolute size, *Int. J. Fract.*, 150, 3-36, 2008.
- [2] D.R. Jones D.R., Eakins D.E., Savinykh A.S., and Razorenov S.V., The effects of axial length on the fracture and fragmentation of expanding rings, *DYMAT 2012, EPJ Web of Conferences* 26, 01032, 2012.
- [3] Mott, N. F., Fragmentation of Shell Cases, *Proceedings of the Royal Society of London A: Mathematical, Physical and Engineering Sciences*, 189 (1018), 300-308, 1947.
- [4] Mock, W. and Holt, W. H., Fragmentation Behavior of Armco Iron and HF-1 Steel Explosive-Filled Cylinders, *J. Appl. Phys*, 54(5), 2344-2351, 1983.
- [5] L.B. Lucy. A numerical approach to the testing of the fission hypothesis. *The Astronomical Journal*, 82(12):1013-1024, 1977.
- [6] R.A. Gingold and J.J. Monaghan. Smoothed particle hydrodynamics: Theory and application to non-spherical stars. *Monthly Notices of the Royal Astronomical Society*, 181:375-389, 1977.
- [7] L.D. Libersky and A.G. Petschek. Smooth Particle Hydrodynamics with strength of materials. In H.E. Trease, M.J. Fritts, and W.P. Crowley, editors, *Advances in the Free-Lagrange Method*, pages 248--257. Springer-Verlag, 1990.
- [8] L.D. Libersky, A.G. Petschek, T.C. Carney, J.R. Hipp, and F.A. Allahdadi. High strain Lagrangian hydrodynamics. *Journal of Computational Physics*, 109:67-75, 1993.
- [9] T. De Vuyst, R. Vignjevic: Total Lagrangian SPH modelling of necking and fracture in electromagnetically driven rings, *International Journal of Fracture*, 180 (1), 53-70, 2013.
- [10] T. De Vuyst, K. Kong, N. Djordjevic, R. Vignjevic, J.C. Campbell, K. Hughes: Numerical modelling of the effect of using multi-explosives on the explosive forming of steel cones, *Journal of Physics: Conference Series*, 734 (3), art. no. 032074, 2016.
- [11] J.I. Lin, *DYNA3D: A Nonlinear, Explicit, Three-Dimensional Finite Element Code for Solid and Structural Mechanics*, User Manual, Lawrence Livermore National Laboratory, California, 2004.